Available online at www.sciencedirect.com
ScienceDirect
Journal of Sound and Vibration 311 (2008) 953–972
JOURNAL OF SOUND AND VIBRATION
www.elsevier.com/locate/jsvi

Influence of crack breathing model on nonlinear dynamics of a cracked rotor

Tejas H. Patel[a], Ashish K. Darpe[b,*]

[a]*Department of Mechanical Engineering, Charotar Institute of Technology, Changa 388421, India*
[b]*Department of Mechanical Engineering, Indian Institute of Technology, Delhi 110016, India*

Received 13 May 2007; received in revised form 5 August 2007; accepted 25 September 2007
Available online 26 October 2007

Abstract

Fatigue cracking of the rotor shaft is an important fault observed in the rotating machinery, which can lead to catastrophic failure. The paper addresses the influence of the crack breathing models on the nonlinear vibration characteristics of the cracked rotors. Nonlinear dynamics of the cracked rotor is investigated using two well-known crack models, i.e. switching crack model and response-dependent breathing crack model. Equations of motion for the cracked rotor are systematically presented for both the models. Through numerical simulations, the dynamic response for both the crack models is compared for the subcritical speed region for the rotor. Distinct differences have been found in bifurcation, amplitude, orbit and Poincaré map when carrying out the comparison between two models for the assumed rotor parameters. Switching crack modelling reveals chaotic, quasi-periodic and subharmonic vibration response for deeper cracks. Rotor system enters into chaos or quasi-periodic motion directly from periodic motion, and leaves the chaos via route of quasi-period. Transient chaos behaviour is also observed for the first time in the case of cracked rotor. Contrary to this, more realistic breathing crack model reveals no evidence of chaotic, quasi-periodic and subsynchronous vibrations in the response. Unbalance eccentricity level and its phase, crack depth and damping are found to have considerable influence on the bifurcation phenomena of the cracked rotor modelled using switching crack model.

1. Introduction

Turbo machinery rotors usually operate in highly stressed conditions and harsh environment. This results in cyclic fatigue, creep, and corrosion. All these physical phenomena lead to generation of fatigue cracks, which can severely damage machine components or even lead to catastrophic failure. Vibration behaviour of cracked structures, in particular cracked rotors has received considerable attention in the last three decades [1,2]. Sabnavis et al. [3] reviewed the research work on crack shaft detection and diagnostics that is published after 1990. Imam et al. [4] developed online rotor crack detection and monitoring system based on measurement of amplitude and phase of $1X$ rev., $2X$ rev. and $3X$ rev. components. Zhou et al. [5] investigated nonlinear dynamic behaviour of the cracked rotor experimentally. They observed higher harmonics (especially $2X$

*Corresponding author.
E-mail address: akdarpe@mech.iitd.ernet.in (A.K. Darpe).

0022-460X/$ - see front matter © 2007 Elsevier Ltd. All rights reserved.
doi:10.1016/j.jsv.2007.09.033

Nomenclature

a	depth of crack
$\bar{a}$	crack depth ratio (a/D)
c	damping coefficient
D	diameter of the shaft
e	dimensionless eccentricity of the unbalance (ε/δ_{st})
E	modulus of elasticity
g_{ij}	flexibility coefficient of the cracked rotor, $i=\xi,\eta$ and $j=\xi,\eta$
$J(\alpha)$	strain energy density function
k_0	stiffness of the uncracked shaft
k_i	direct stiffness coefficient, $i=y,z,\xi,\eta$
k_{ij}	cross stiffness coefficient, $i=y,z,\xi,\eta$ and $j=y,z,\xi,\eta$
$\hat{k}_i$	stiffness of cracked rotor in ith direction, $i=\xi,\eta$
K^I	total stress intensity factor
L	length of shaft
m	mass of the disc
p	rotational speed ratio
Q_i	lateral forces at the crack location in ith direction, $i=\xi,\eta$
r_i	speed ratio, where $r_i=\omega_i/\omega$, $i=0,\xi,\eta,\xi\eta$
T	coordinate transformation matrix
u_i	deflection due to crack, $i=\xi,\eta$
Y, Z	rotor response in vertical and horizontal direction, respectively
Y–Z	stationary coordinate system
$\bar{Y},\bar{Z}$	dimensionless rotor response in vertical and horizontal direction, respectively
α	depth of crack at any distance, w
β	orientation of unbalance relative to the crack direction (x)
δ_{st}	static deflection of the uncracked rotor
Δk_i	stiffness variation in the cracked rotor along ith direction, $i=\xi,\eta$
ε	eccentricity of centre of mass at the disc
ν	Poisson's ratio
σ_i	stress acting at a point along the crack edge along ith direction, $i=\xi,\eta$
θ	angle of rotation
τ	dimensionless time
ω	rotational speed
ω_0	bending natural frequency of the uncracked rotor
ω_i	natural frequencies of the cracked shaft along ith direction, $i=\xi,\eta,\xi\eta$
ξ–η	rotor fixed coordinate system
ζ	damping factor

frequency component) in the response of the cracked rotor, when rotor is running in the subcrticial speed range. Several researchers focused their studies mainly on unbalance vibration response of the cracked rotors [6,7], while others [8–10] studied coupling of the vibrations due to presence of crack. Recently, Quinn et al. [11] demonstrated theoretically and experimentally the use of active magnetic bearing as a force actuator for health monitoring of the rotor dynamic systems in presence of breathing shaft cracks. It is well-established from the literature [4–7] that along with increase in $1X$ response, rotor crack induces higher harmonic, particularly $2X$ and $3X$ components, due to breathing of the crack under gravity loading.

Cracked rotor is highly nonlinear system. Recently, a few of the studies on oscillations induced by crack have indicated that besides well-known super-harmonic response, chaotic [12,13,15–17] and quasi-periodic [14,15] motions are also possible. Muller et al. [12] applied theory of Lyapunov exponents to non-smooth dynamical system with a cracked rotor, and found the chaotic motion and strange attractors. Pu et al. [13] introduced nonlinear effect of a crack considering the crack as an external force. The nonlinear forces were reconstructed using the state space theory. From the numerical simulations, bifurcation and chaos were observed. Period doubling and triple period bifurcations were noted in some of the cases. Considering the crack as an external disturbance described by a series of trigonometric function, Pu et al. [14] observed quasi-periodic vibrations in another study. Qin et al. [15] noted chaotic vibrations with increase in crack depth, in some range of the speed. Routes to chaos included intermittence and quasi-period. They noted no effect of the crack angle with respect to the unbalance on chaotic behaviour of cracked rotor. In another study, Qin et al. [16] examined grazing bifurcation in the response of the cracked rotor. Yiming et al. [17] found critical condition for the chaotic states using Melnikov function corresponding to homoclinic orbits.

In all the previous studies that showed presence of chaotic and quasi-periodic vibrations [12–17], the common aspect is the modelling of breathing of crack. These studies are made using the switching crack model. Crack

breathing in rotors is often simulated using two well-known models. One is the switching crack model (also known as hinge model), in which the stiffness of the rotor switches from one corresponding to the closed crack (uncracked shaft stiffness) to the stiffness corresponding to the fully open crack state. Gasch [18] has introduced this simple hinge model to simulate the breathing behaviour of the crack. He used the sign of the response in rotor fixed coordinate system in the switching function that governs change in stiffness. The other model is the response-dependent breathing crack model, proposed by Jun et al. [6]. This model iteratively estimates the status of the crack closure using forces acting on the crack section, and thereby evaluates the stiffness of the cracked section. In this way, the model accounts for partial opening/closing of crack. Since in real rotors, the stiffness variation is likely to be gradual; the assumption of abrupt sudden stiffness switching is not appropriate. Hence, the response-dependant breathing crack model should be used to emulate the true breathing behaviour of the cracked rotors.

Darpe et al. [19] investigated numerically and experimentally, the differences in the transient response of the cracked rotor during passage through subharmonic resonances. Using different crack models, they found differences in amplitudes of higher harmonic components at subharmonic resonances. Although a few research studies [12–17] reported the chaotic/quasi-periodic vibration in rotors with crack, the studies are mainly confined to the numerical simulations and no experimental or field observation of these vibration features were reported by any researchers. This is also confirmed by extensive literature review articles [1–3]. Secondly, all these studies on chaotic and quasi-periodic vibrations of the cracked rotor have used elementary crack model (i.e. switching crack model) in the analysis. It is therefore, necessary to scrutinize and compare the nonlinear behaviour of cracked rotor using both the crack models, i.e. switching crack model and response-dependent breathing crack model. In the present study, nonlinear dynamics of the cracked rotor is explored. The analysis includes the detailed study related to bifurcation characteristics, chaotic and quasi-periodic vibrations for the cracked rotor for the speeds below the bending critical speed of the rotor. Two degrees of freedom, flexible cracked Jeffcott rotor model on simple rigid supports is used for numerical simulations. The equations of motion are presented for both the crack models, i.e. switching crack model and breathing crack model. The nonlinear vibration characteristic of the cracked rotor is investigated and compared for both the models, which was not attempted before. Several new findings have been reported and significance of using more realistic crack model is outlined.

2. Crack breathing models

2.1. Equations of motion

Jeffcott rotor is considered mounted on rigid bearing supports having a disk of mass m at the centre of the shaft of length L. A transverse surface crack of depth a, is assumed at the midspan of the rotor. The crack is assumed to have a straight edge. Let Y and Z are the fixed coordinates and ξ and η are the rotating coordinates in the crack cross section. ξ is the weak crack direction and η is the strong crack direction (Fig. 1(a)). The disk is having unbalance eccentricity ε oriented at an angle β with the weak crack direction. $\theta(t)$ is the instantaneous angle of rotation and ω is the rotor speed. The equations of motion for the cracked Jeffcott rotor, can be written in fixed coordinate Y–Z system (Fig. 1(a)) as

$$\begin{aligned} m\ddot{Y} + c\dot{Y} + k_y Y + k_{yz} Z &= m\varepsilon\omega^2 \cos(\theta+\beta) - mg, \\ m\ddot{Z} + c\dot{Z} + k_{zy} Y + k_z Z &= m\varepsilon\omega^2 \sin(\theta+\beta). \end{aligned} \tag{1}$$

Breathing crack model and switching crack model differ from each other. In breathing crack model, amount of open part of the crack continuously changes with the shaft rotation, thereby accounting partial open/close state of the crack. In contrast, in the switching crack model, the crack is assumed to be in either fully open state or fully close state. Partial opening and closing of the crack is not accounted. The two commonly used crack models used in the present analysis are briefed below for the sake of completeness.

2.2. Breathing crack model

The stiffness coefficients of Eq. (1) in the fixed coordinate system can be obtained from the stiffness coefficients k_ξ, k_η, $k_{\xi\eta}$ and $k_{\eta\xi}$ defined in the rotational frame ξ–η, by proper transformation

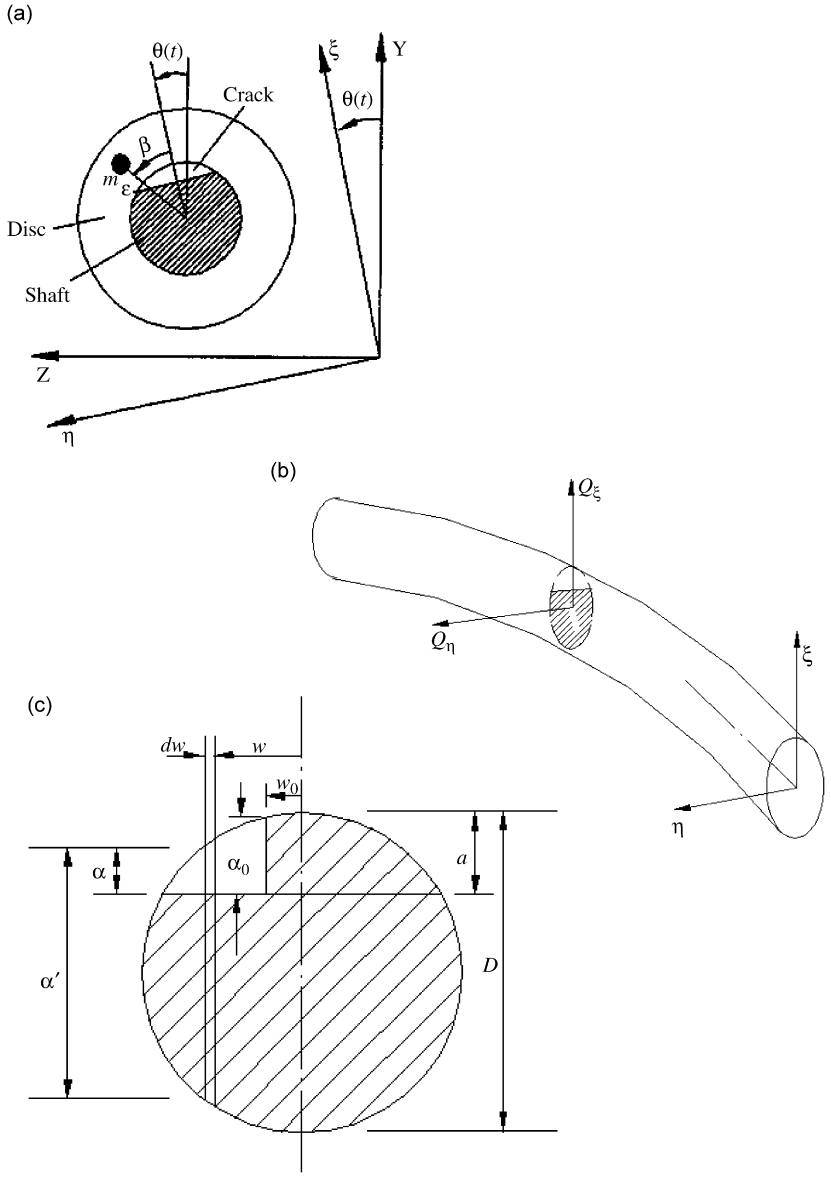

Fig. 1. (a) Coordinate system, (b) forces acting at the crack location, and (c) cross-section at crack location [20].

matrix. As breathing crack model considers partial opening and closing of the crack during shaft rotation, the cross stiffness terms $k_{\xi\eta}$ and $k_{\eta\xi}$ appear in the equations of motion (Eq. (1)), and, $k_{\xi\eta}$ is equal to $k_{\eta\xi}$.

$$\begin{bmatrix} k_y & k_{yz} \\ k_{zy} & k_z \end{bmatrix} = T^{-1} \begin{bmatrix} k_\xi & k_{\xi\eta} \\ k_{\eta\xi} & k_\eta \end{bmatrix} T, \tag{2}$$

where the transformation matrix is

$$T = \begin{bmatrix} \cos\theta & \sin\theta \\ -\sin\theta & \cos\theta \end{bmatrix}.$$

The equations of motion can be rewritten as

$$\begin{aligned} &m\ddot{Y} + c\dot{Y} + \tfrac{1}{2}\{k_\xi + k_\eta + (k_\xi - k_\eta)\cos 2\theta - 2k_{\xi\eta}\sin 2\theta\}Y + \tfrac{1}{2}\{(k_\xi - k_\eta)\sin 2\theta + 2k_{\xi\eta}\cos 2\theta\}Z \\ &\quad = m\varepsilon\omega^2\cos(\theta+\beta) - mg, \\ &m\ddot{Z} + c\dot{Z} + \tfrac{1}{2}\{k_\xi + k_\eta + (k_\eta - k_\xi)\cos 2\theta + 2k_{\xi\eta}\sin 2\theta\}Z + \tfrac{1}{2}\{(k_\xi - k_\eta)\sin 2\theta + 2k_{\xi\eta}\cos 2\theta\}Y \\ &\quad = m\varepsilon\omega^2\sin(\theta+\beta). \end{aligned} \tag{3}$$

Stiffness coefficients k_ξ, k_η, $k_{\xi\eta}$ and $k_{\eta\xi}$ are computed from flexibilities of the cracked shaft [6,20]. Total flexibility of the shaft is made up of two parts: one is the uncracked shaft flexibility and second is the additional flexibility introduced by the crack. The amount of flexibility changes with the amount of the open part of the crack. As the rotor rotates, the crack breathes. The amount of open part of the crack constantly changes, thereby changing the flexibility of the cracked rotor. In this way the model accounts for partial opening and closing of the crack. The cross stiffness terms $k_{\xi\eta}$ and $k_{\eta\xi}$ appear due to partial opening of the crack. The flexibility due to crack is

$$g_{ij} = \frac{\partial u_i}{\partial Q_j}, \tag{4}$$

where $i = \xi,\ \eta$ and $j = \xi,\ \eta$, $Q =$ force acting on the crack cross-section (Fig. 1(b)), u_i is the additional deflection due to presence of crack and is given as [21]

$$u_i = \frac{\partial}{\partial Q_i}\left[\int J(\alpha)\,\mathrm{d}\alpha\right]. \tag{5}$$

$J(\alpha)$ is the strain energy density function given by

$$J(\alpha) = \frac{1}{E}(K^I)^2, \tag{6}$$

where K^I is the total stress intensity factor (SIF), which is expressed as follows:

$$K^I = K^I_{Q_\xi} + K^I_{Q_\eta}. \tag{7}$$

Here,

$$K^I_{Q_\xi} = \sigma_\xi\sqrt{\pi\alpha}F(\alpha/\alpha'), \quad K^I_{Q_\eta} = \sigma_\eta\sqrt{\pi\alpha}F'(\alpha/\alpha') \tag{8}$$

are the opening mode (mode I) stress intensity factors (SIFs) due to Q_ξ and Q_η respectively. Q_ξ and Q_η are the lateral forces at the crack location, as shown in Fig. 1(b). It may be noted that owing to pure bending assumption, effect of shear deformation is not taken into account. Also since torsional effects are not considered, cracking in modes II and III involving shear stresses is not present.

σ_ξ and σ_η are the bending stresses due to Q_ξ and Q_η, respectively. They are given by

$$\sigma_\xi(w) = \frac{(Q_\xi L/4)(\alpha'/2)}{I}, \quad \sigma_\eta(w) = \frac{(Q_\eta L/4)w}{I}, \tag{9}$$

where $I = (\pi D^4/64)$, $\alpha' = \sqrt{D^2 - (2w)^2}$ and

$$Q_\xi = k_\xi\xi + k_{\xi\eta}\eta, \quad Q_\eta = k_{\eta\xi}\xi + k_\eta\eta. \tag{10}$$

It can be noted that the SIF is a function of forces acting on the rotor at the crack location (Fig. 1(b)) and the position along the crack edge, w (Fig. 1(c)). The forces Q_ξ and Q_η in turn depend on the rotor response (ξ, η) (see Eq. (10)). The stiffness and response are interdependent and equations are thus nonlinear.

The relation between rotating coordinates and fixed coordinates is given by

$$\begin{Bmatrix} \xi \\ \eta \end{Bmatrix} = \begin{bmatrix} \cos\theta & -\sin\theta \\ \sin\theta & \cos\theta \end{bmatrix} \begin{Bmatrix} Y \\ Z \end{Bmatrix}. \tag{11}$$

The functions F and F' in Eq. (8) are given by

$$F(\alpha/\alpha') = \sqrt{\frac{2\alpha'}{\pi\alpha}\tan\left(\frac{\pi\alpha}{2\alpha'}\right)}\,\frac{0.923 + 0.199[1-\sin(\pi\alpha/2\alpha')]^4}{\cos(\pi\alpha/2\alpha')}, \tag{12}$$

$$F'(\alpha/\alpha') = \sqrt{\frac{2\alpha'}{\pi\alpha}\tan\left(\frac{\pi\alpha}{2\alpha'}\right)}\,\frac{0.752 + 2.02(\alpha/\alpha') + 0.37[1-\sin(\pi\alpha/2\alpha')]^3}{\cos(\pi\alpha/2\alpha')}. \tag{13}$$

Using Eqs. (4)–(13), the total flexibilities of the cracked shaft can be written as

$$\begin{aligned} g_\xi &= \frac{L^3}{48EI} + \iint \frac{128L^2\alpha'^2\alpha}{E\pi D^8} F(\alpha/\alpha')^2\,\mathrm{d}\alpha\,\mathrm{d}w,\\ g_\eta &= \frac{L^3}{48EI} + \iint \frac{512L^2w^2\alpha}{E\pi D^8} F'(\alpha/\alpha')^2\,\mathrm{d}\alpha\,\mathrm{d}w,\\ g_{\xi\eta} &= g_{\eta\xi} = \iint \frac{256L^2\alpha'^2w}{E\pi D^8}\alpha F(\alpha/\alpha')F'(\alpha/\alpha')\,\mathrm{d}\alpha\,\mathrm{d}w. \end{aligned} \tag{14}$$

The term $L^3/48EI$ represents the flexibility of the uncracked shaft. It is important to note that the integration limits in above expressions are from 0 to α for depth of crack and the limits for width are not specified. The limits of integration on width depend on the open part of the crack, which can be obtained from the sign of SIF along the crack edge. After finding the total SIF (Eq. (7)) at various locations on crack edge, the position where SIF changes the sign can be found out. The positive SIF indicates the tensile stress field and the crack in open state, whereas, negative SIF indicates compressive stress field and the crack in close state. Once the amount of open part is known, the integration can be performed for the open part of the crack.

Using the above flexibility values, stiffness coefficients in the rotational frame of reference are obtained, as follows:

$$k_\xi = \frac{g_\eta}{g_\xi g_\eta - g_{\xi\eta}^2}, \quad k_\eta = \frac{g_\xi}{g_\xi g_\eta - g_{\xi\eta}^2}, \quad k_{\xi\eta} = k_{\eta\xi} = \frac{-g_{\xi\eta}}{g_\xi g_\eta - g_{\xi\eta}^2}. \tag{15}$$

It should be noted that the above stiffness values change as the rotor rotates, due to opening/closing of the crack with rotation under gravity influence. From the sign of SIF along the crack edge, open part of the crack is found out, which in turn used to get new flexibilities (Eq. (14)) and hence new stiffness values (Eq. (15)). These new stiffness values are used back again in the equations of motion (Eq. (3)) to obtain new set of rotor response (ξ, η) that is again used to estimate new stiffness values. Thus the equations of motion are nonlinear.

Equations of motion (Eq. (3)) can be non-dimensionalized using following non-dimensional parameters:

$$\begin{aligned} &\bar{Y} = Y/\delta_{\mathrm{st}}, \quad \bar{Z} = Z/\delta_{\mathrm{st}}, \quad \zeta = \frac{c}{2\sqrt{k_0 m}}, \quad \tau = \omega t, \quad e = \varepsilon/\delta_{\mathrm{st}}, \quad \bar{a} = a/D, \quad r_0 = \omega_0/\omega,\\ &r_\xi = \omega_\xi/\omega, \quad r_\eta = \omega_\eta/\omega, \quad r_{\mathrm{unb}} = \omega/\omega_0, \quad r_{\xi\eta} = \omega_{\xi\eta}/\omega, \quad r_{\eta\xi} = \omega_{\eta\xi}/\omega, \end{aligned} \tag{16}$$

where

$$\delta_{\mathrm{st}} = mg/k_0, \quad \omega_0 = \sqrt{\frac{k_0}{m}}, \quad \omega_\xi = \sqrt{\frac{k_\xi}{m}}, \quad \omega_\eta = \sqrt{\frac{k_\eta}{m}}, \quad \omega_{\xi\eta} = \sqrt{\frac{k_{\xi\eta}}{m}}, \quad \omega_{\eta\xi} = \sqrt{\frac{k_{\eta\xi}}{m}}.$$

Here, k_0 is the stiffness of the shaft without crack. Equations of motion in non-dimensional form are

$$\begin{aligned} &\ddot{\bar{Y}} + 2\zeta r_0\dot{\bar{Y}} + \tfrac{1}{2}\left\{r_\xi^2 + r_\eta^2 + (r_\xi^2 - r_\eta^2)\cos 2\tau - 2r_{\xi\eta}^2 \sin 2\tau\right\}\bar{Y}\\ &\quad + \tfrac{1}{2}\left\{(r_\xi^2 - r_\eta^2)\sin 2\tau + 2r_{\xi\eta}^2 \cos 2\tau\right\}\bar{Z} = e\cos(\tau+\beta) - r_0^2,\\ &\ddot{\bar{Z}} + 2\zeta r_0\dot{\bar{Z}} + \tfrac{1}{2}\left\{r_\xi^2 + r_\eta^2 + (r_\eta^2 - r_\xi^2)\cos 2\tau + 2r_{\xi\eta}^2 \sin 2\tau\right\}\bar{Z}\\ &\quad + \tfrac{1}{2}\left\{(r_\xi^2 - r_\eta^2)\sin 2\tau + 2r_{\xi\eta}^2 \cos 2\tau\right\}\bar{Y} = e\sin(\tau+\beta). \end{aligned} \tag{17}$$

2.3. Switching crack model

In switching crack model, the crack remains either fully open or fully closed. Hence, partial opening and closing of the crack is absent. So, the cross-coupled stiffness terms vanish and direct stiffness possesses bi-levels. Here stiffness coefficients of Eq. (1) are obtained from the stiffness coefficients k_ξ, k_η defined in the rotational frame $\xi-\eta$ by transformation matrix. The stiffness matrix in the rotational frame is as follows:

$$\begin{bmatrix} k_\xi & 0 \\ 0 & k_\eta \end{bmatrix} = \begin{bmatrix} k_0 & 0 \\ 0 & k_0 \end{bmatrix} - \Theta \begin{bmatrix} \Delta k_\xi & 0 \\ 0 & \Delta k_\eta \end{bmatrix}, \tag{18}$$

where stiffness k_0 represents uncracked shaft stiffness. Δk_ξ, Δk_η are the stiffness variations in the ξ-axis (weak direction) and η-axis (strong direction) respectively:

$$\Delta k_\xi = k_0 - \hat{k}_\xi, \quad \Delta k_\eta = k_0 - \hat{k}_\eta \tag{19}$$

Stiffnesses $\hat{k}_\xi$ and $\hat{k}_\eta$ are the stiffnesses in the weak direction (ξ-axis) and strong direction (η-axis) respectively, at fully open state of the crack.

Θ is the switching function which switches from 1 to 0 for fully open crack to fully close crack respectively. It depends on the response ξ. It is assumed that when the response of rotor centre along weak crack direction ξ is positive, the crack is assumed to be open and closed when it is negative. Thus,

$$\Theta = \begin{cases} 1 & \text{for} \quad \xi > 0, \\ 0 & \text{for} \quad \xi \leqslant 0. \end{cases} \tag{20}$$

When the response ξ is positive, the crack is fully open and the stiffnesses in ξ and η directions are equal to $\hat{k}_\xi$ and $\hat{k}_\eta$, respectively. Otherwise, the stiffnesses in ξ and η directions correspond to the uncracked rotor stiffness k_0.

The equations of motion for the cracked Jeffcott rotor using switching crack model can be written as follows:

$$\begin{aligned} &m\ddot{Y} + c\dot{Y} + \left[k_0 - \tfrac{1}{2}\Theta\left\{2k_0 - \hat{k}_\xi - \hat{k}_\eta + \left(\hat{k}_\eta - \hat{k}_\xi\right)\cos 2\theta\right\}\right] Y - \tfrac{1}{2}\Theta\left\{\left(\hat{k}_\eta - \hat{k}_\xi\right)\sin 2\theta\right\} Z \\ &\quad = m\varepsilon\omega^2 \cos(\theta+\beta) - mg, \\ &m\ddot{Z} + c\dot{Z} + \left[k_0 - \tfrac{1}{2}\Theta\left\{2k_0 - \hat{k}_\xi - \hat{k}_\eta - \left(\hat{k}_\eta - \hat{k}_\xi\right)\cos 2\theta\right\}\right] Z - \tfrac{1}{2}\Theta\left\{\left(\hat{k}_\eta - \hat{k}_\xi\right)\sin 2\theta\right\} Y \\ &\quad = m\varepsilon\omega^2 \sin(\theta+\beta). \end{aligned} \tag{21}$$

The above equations can be written in the dimensionless form, using following non-dimensional parameters:

$$\begin{aligned} &\bar{Y} = Y/\delta_{\mathrm{st}}, \quad \bar{Z} = Z/\delta_{\mathrm{st}}, \quad \zeta = \frac{c}{2\sqrt{k_0 m}}, \quad \tau = \omega t, \quad e = \varepsilon/\delta_{\mathrm{st}}, \\ &\bar{a} = a/D, \quad r_0 = \omega_0/\omega, \ \ r_\xi = \omega_\xi/\omega, \ \ r_\eta = \omega_\eta/\omega, \end{aligned} \tag{22}$$

where

$$\delta_{\mathrm{st}} = mg/k_0, \quad \omega_0 = \sqrt{\frac{k_0}{m}}, \quad \omega_\xi = \sqrt{\frac{\hat{k}_\xi}{m}}, \quad \omega_\eta = \sqrt{\frac{\hat{k}_\eta}{m}}.$$

Equations of motion in dimensionless form are

$$\begin{aligned} &\ddot{\bar{Y}} + 2\zeta r_0 \dot{\bar{Y}} + \left[r_0^2 - \tfrac{1}{2}\Theta\left\{2r_0^2 - r_\xi^2 - r_\eta^2 + \left(r_\eta^2 - r_\xi^2\right)\cos 2\tau\right\}\right] \bar{Y} - \tfrac{1}{2}\Theta\left\{\left(r_\eta^2 - r_\xi^2\right)\sin 2\tau\right\} \bar{Z} = e\cos(\tau+\beta) - r_0^2, \\ &\ddot{\bar{Z}} + 2\zeta r_0 \dot{\bar{Z}} + \left[r_0^2 - \tfrac{1}{2}\Theta\left\{2r_0^2 - r_\xi^2 - r_\eta^2 - \left(r_\eta^2 - r_\xi^2\right)\cos 2\tau\right\}\right] \bar{Z} - \tfrac{1}{2}\Theta\left\{\left(r_\eta^2 - r_\xi^2\right)\sin 2\tau\right\} \bar{Y} = e\sin(\tau+\beta). \end{aligned} \tag{23}$$

The non-dimensionalized equations of motion (Eqs. (17) and (23)) are solved using Runge–Kutta fourth-order numerical integration method. Relatively small time step and long time marching technique is adopted to obtain the stabilized steady-state response. Using both the crack models and following rotor configuration,

the dynamic response is studied using bifurcation diagram, orbit plot and Poincaré map. Physical rotor parameters used for the simulations are as follows: shaft diameter, $D = 45$ mm; length, $L = 0.7$ m; disk mass, $m = 25$ kg; damping factor, $\zeta = 0.01$; rotor crack depth ratio, $a/D = 0.2$, 0.35 and 0.44 (i.e. 9, 15.75 and 19.80 mm, respectively); unbalance eccentricity, $e = 0.2042$ and 4.0826 (i.e. $\varepsilon =$ 1e−05 m and 2e−04 m, respectively).

In a nonlinear system, alteration in the parameters can change the stability of the equilibrium points, as well as numbers of equilibrium points. Study of all such changes is made using bifurcation diagram. For the numerical computation of a bifurcation diagram, one of the rotor parameters such as speed, damping, etc. is increased (decreased) in a constant step and the state variables at the end of the integration are used as the initial values for the next parameter value. This means that there is a tendency for the integration to follow a single response curve. The Y-coordinate of the return point in the Poincaré section is then plotted versus the rotor parameter to get bifurcation diagram. The orbit plot, which is essentially the movement of the rotor centre in YZ plane, is drawn with vibration data of last 50 cycles of the steady-state response. A Poincaré section is the stroboscopic picture of motion taken at some particular phase of the forcing motion. To draw, a Poincaré map vibration data of first 500 cycles are discarded and the data of next 3000 cycles are used. To get the qualitative insight, the results are shown in the dimensionless parameters (i.e. X/δ_{st}, Y/δ_{st}, etc.).

3. Results and discussion

In this section nonlinear behaviour of the cracked rotor is examined. Most of the previous studies [13,15,16] on the bifurcation characteristics have been undertaken using rotational speed as control parameter. However, the other rotor parameters such as damping, unbalance level and phase also have significance in the nonlinear behaviour of the cracked rotor. Therefore, study of the effect of these parameters on nonlinear dynamic response has been undertaken in the present work. Bifurcation properties of the cracked rotors are examined using rotation speed, damping, unbalance phase as the control parameters. In each of the following subsections, results using switching crack model are discussed first and then compared with the results obtained from breathing crack model.

3.1. Effect of speed of rotation

Bifurcation diagram is obtained by solving equations of motion over the running speed range 44–350 rad s^{-1} (i.e. 420.17–3342.25 rev min^{-1}), in increments of 1.57 rad s^{-1}. It is important that the response data corresponds to fully stabilized rotor motion. Hence, the simulation is continued for 500 rotations at each speed. Out of 500 rotations, data of only last 100 cycles are used in plotting the bifurcation diagram. Simulation for more number of cycles did not result in any improvement in the result. The simulations are run for different levels of unbalance.

3.1.1. Low level of unbalance

Fig. 2 provides the bifurcation behaviour of the cracked rotor ($a/D = 0.44$, $e = 0.2042$, $\beta = 90^\circ$) using switching crack model. The rotating speed ratio ($p = 1/r_0 = \omega/\omega_0$) is taken as the control parameter, which is defined as the ratio of rotation speed to the natural frequency of the uncracked rotor (ω_0). The data of Fig. 2(a) is plotted in Fig. 2(b) for smaller speed range, $p = 0.10$–0.44. It can be seen from Fig. 2 that the rotor motion experiences frequent change from one equilibrium value to another equilibrium value at p equal to 0.1018, 0.1159, 0.1334, 0.1545, 0.1861, 0.2352, 0.309 and 0.4634. In fact, these speed ratios are very close to $\frac{1}{9}$, $\frac{1}{8}$, $\frac{1}{7}$, $\frac{1}{6}$, $\frac{1}{5}$, $\frac{1}{4}$, $\frac{1}{3}$ and $\frac{1}{2}$ times the bending critical of cracked rotor (i.e. ω_η, where $\omega_\eta = \sqrt{k_\eta/m}$), respectively. This means cracked rotor experience change from one steady-state value to another at all integer submultiples of the critical speed in the considered speed range. It may be noted that the vibration response experiences phase change at subharmonic resonances at submultiples of the critical speed.

As the speed increases, the motion is synchronous with period one till rotation speed ratio (p) reaches 0.4809, where vibration motion bifurcated directly to chaotic, from the periodic motion. Fig. 3(i) is the orbit plot and Poincaré map of the motion at this speed ratio. Scattered attractors in the Poincaré map suggest

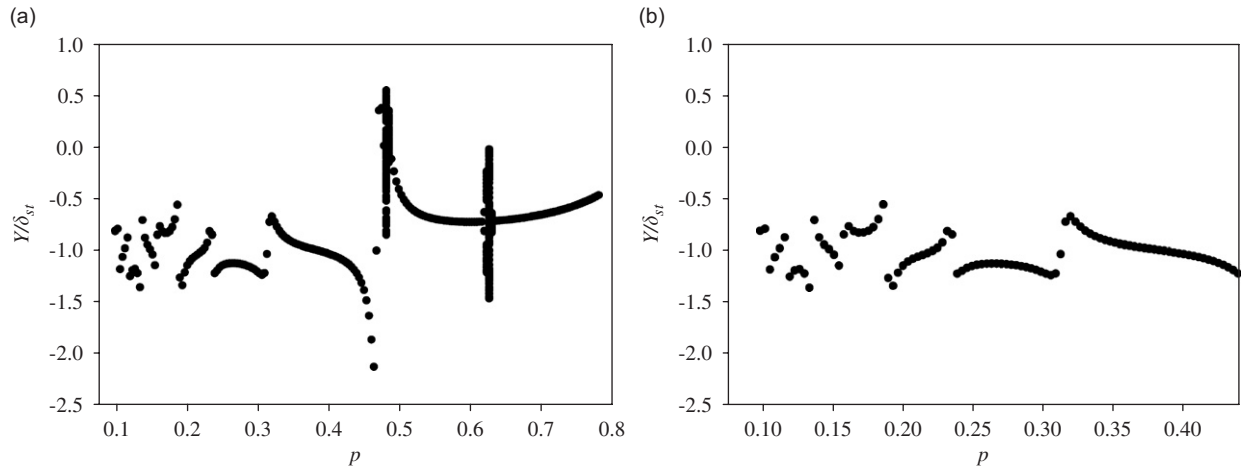

Fig. 2. Bifurcation diagram of switching crack model, $a/D = 0.44$, $e = 0.2042$, $\beta = 90^\circ$. (a) $p = 0.10$ to 0.78, (b) $p = 0.10$ to 0.44.

chaotic behaviour of the vibration motion. It may be noted from Fig. 3(a)(i) that, though the motion is chaotic, rotor centre orbits close to some periodic or regular orbit. The response becomes quasi-periodic immediately at next speed ratio, $p = 0.4844$, as depicted from the closed curve in Poincaré map of Fig. 3(ii). The motion immediately returns to periodic one at subsequent speed step. The rotor thus enters into chaotic state from period one motion and leaves the chaos via route of quasi-periodic motion. Next bifurcation takes place at $p = 0.6189$, where period one motion changes to period two motion. The vibration becomes period 30 at $p = 0.6224$ (refer Fig. 3(iii)), and then quasi-periodic till $p = 0.6295$. The motion remains period one then onwards.

It can be noted here that at higher crack depth and low level of unbalance, switching crack model exhibit chaotic, quasi-periodic and subharmonic vibrations for a small speed range. Routes in and out of chaos include direct chaos from periodic motion and quasi-periodic motion, respectively.

The bifurcation behaviour of the cracked rotor with response-dependent breathing crack model for the same rotor parameters ($a/D = 0.44$, $e = 0.2042$, $\beta = 90^\circ$) is shown in Fig. 4. Similar to switching crack model (Fig. 2), the rotor response in this case also jump from one equilibrium state to another at submultiples (i.e. $\frac{1}{2}$, $\frac{1}{3}$, $\frac{1}{4}$, etc.) of the bending critical of cracked rotor. However, jump for switching crack model is much more compared to breathing crack model, except near half the bending critical speed. It can be seen from the bifurcation diagram that breathing crack model displays synchronous periodic motion. Comparison of the orbital plots and Poincaré sections obtained using both the crack models would disclose the difference in dynamic behaviour of both the crack models. Fig. 5 shows the rotor orbits and Poincaré sections at rotor speed ratios 0.4809, 0.4844 and 0.6224. There is only one point in the each of the Poincaré maps, which proves the period one response. Contrary to this, the switching crack model reveal chaotic, quasi-periodic and subharmonic (period 30) motion (refer Fig. 3) at speed ratios 0.4809, 0.4844 and 0.6224, respectively, for the same rotor parameters.

3.1.2. High level of unbalance

The study of the bifurcation phenomena at high value of unbalance is undertaken for dimensionless unbalance eccentricity, $e = 4.0826$. Fig. 6 shows bifurcation behaviour of the cracked rotor ($a/D = 0.44$, $\beta = 90^\circ$) using switching crack model. Fig. 6(b) shows the response in speed range $p = 0.55$–0.68. Apart from frequent switching from one equilibrium value to another at integer submultiples of the critical speeds, the rotor response displays rich quasi-periodic vibrations. Quasi-period character in vibration motion appear first at $p = 0.316$ (i.e. near one-third bending natural frequency of the cracked rotor). Fig. 7(i) is the orbit plot and Poincaré map of the rotor response at $p = 0.316$, which reveals the quasi-periodic motion. The motion immediately becomes periodic and remains periodic until speed ratio reaches to a value 0.4699 (i.e. near one-half bending natural frequency of the cracked rotor). Fig. 7(ii) is the orbit plot and Poincaré map of the rotor

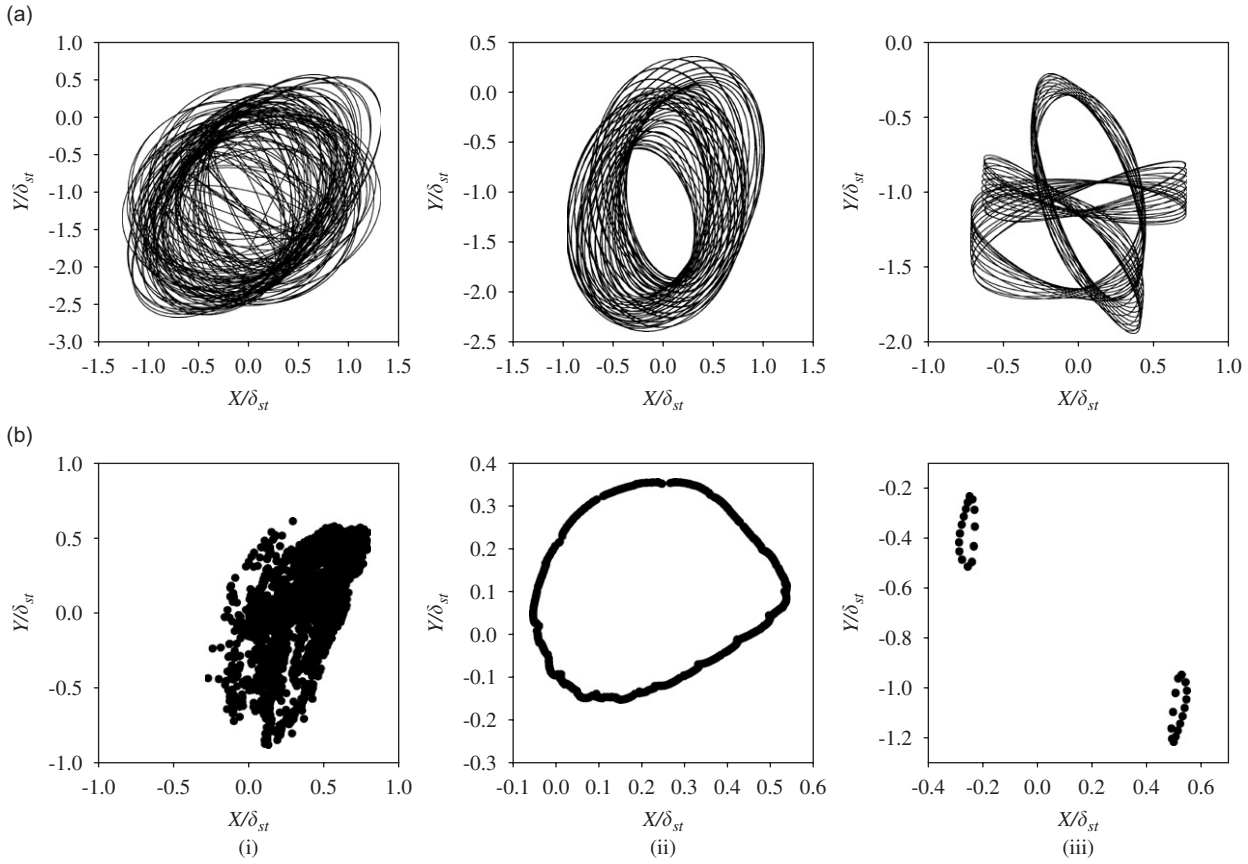

Fig. 3. (a) Orbit plots and (b) Poincaré maps at (i) $p = 0.4809$, (ii) $p = 0.4844$, (iii) $p = 0.6224$; switching crack model, $a/D = 0.44$, $e = 0.2042$, $\beta = 90^\circ$.

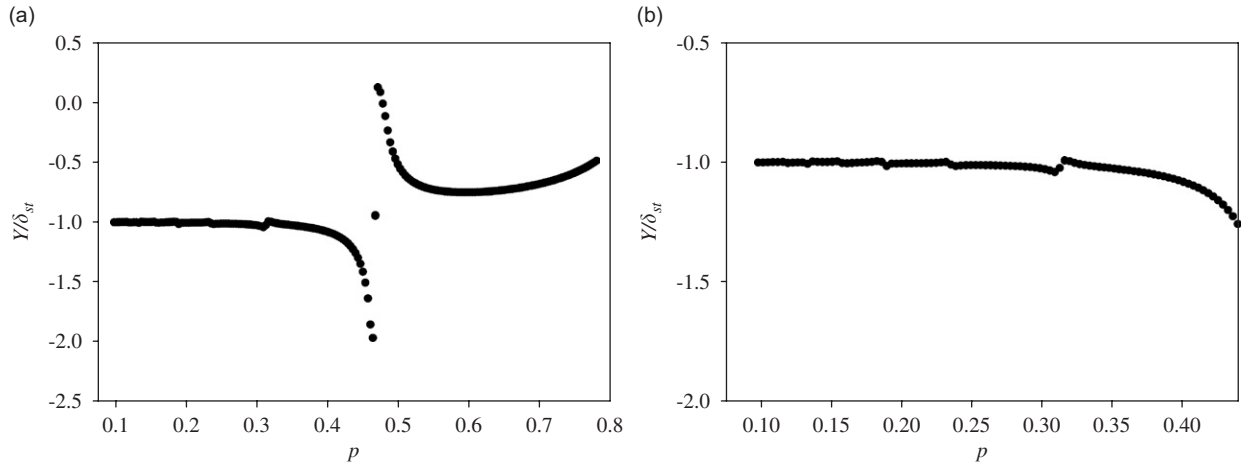

Fig. 4. Bifurcation diagram of breathing crack model, $a/D = 0.44$, $e = 0.2042$, $\beta = 90^\circ$. (a) $p = 0.10$ to 0.78, (b) $p = 0.10$ to 0.44.

response at $p = 0.4699$. The motion remains quasi-periodic then onwards until $p = 0.6735$. At this speed, rotor system bifurcates to period eight motion (see Fig. 7(iii)). Eight discrete points in the Poincaré section indicates period eight movement of the rotor. Vibration motion immediately becomes quasi-periodic at next speed ratio

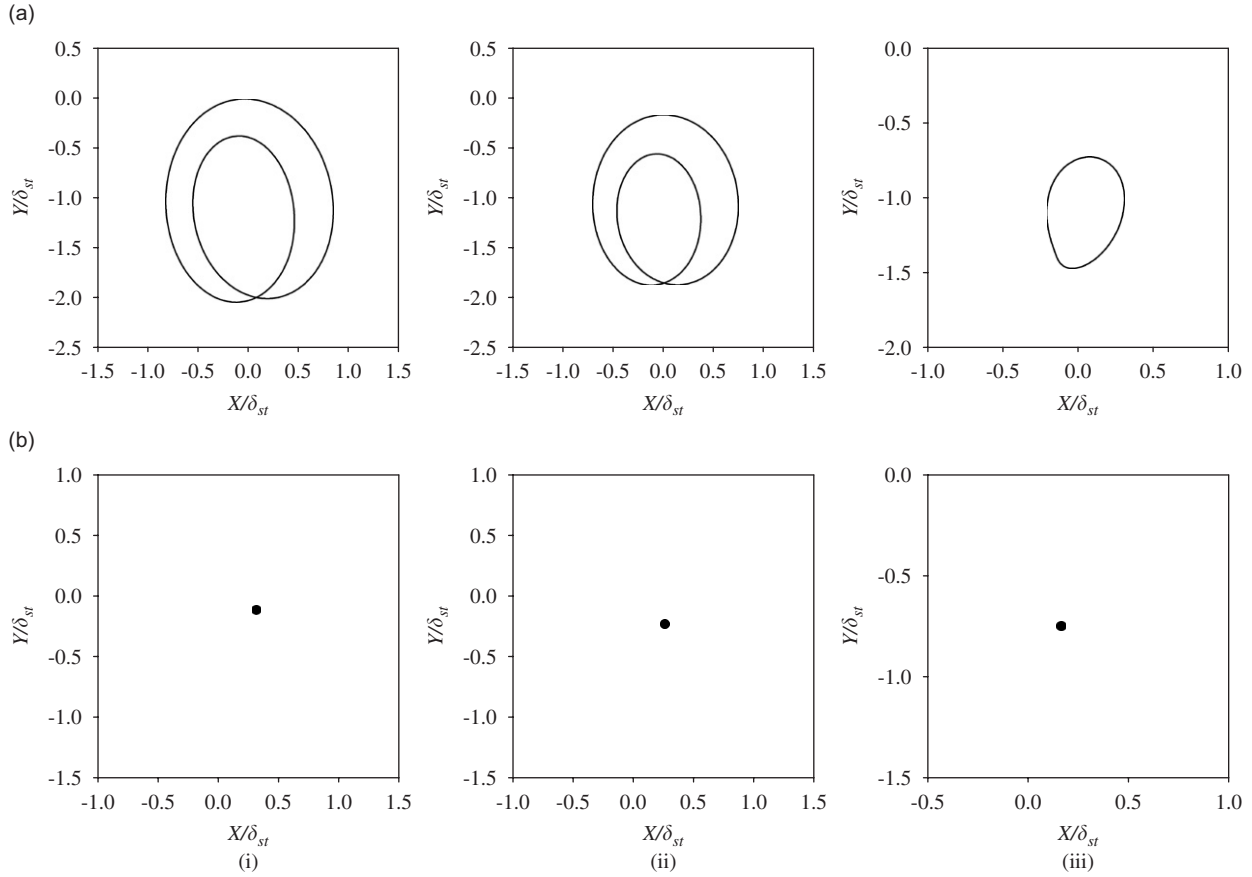

Fig. 5. (a) Orbit plots and (b) Poincaré maps at (i) $p = 0.4809$, (ii) $p = 0.4844$, (iii) $p = 0.6224$; breathing crack model, $a/D = 0.44$, $e = 0.2042$, $\beta = 90^\circ$.

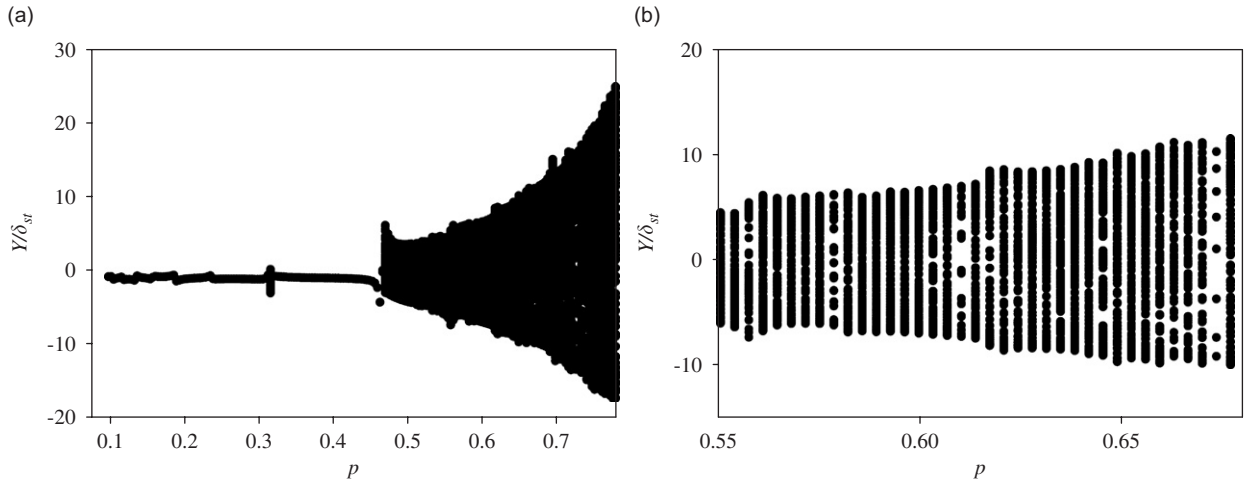

Fig. 6. Bifurcation diagram of switching crack model, $a/D = 0.44$, $e = 4.0286$, $\beta = 90^\circ$. (a) $p = 0.10$ to 0.78, (b) $p = 0.55$ to 0.68.

value, i.e. $p = 0.677$. The vibration response remains quasi-periodic then onwards. In this way, the cracked rotor modelled with switching crack model, exhibit rich form of quasi-periodic vibrations, at higher level of unbalance compared to lower level of unbalance (Fig. 2(a)).

Fig. 8 reveals the bifurcation phenomenon of the cracked rotor with breathing crack model, for the same rotor parameters. Contrary to the switching crack model, the bifurcation diagram indicates period one motion for the entire speed range.

The above study of effect of unbalance level on the bifurcation phenomena of the cracked rotor imply that the rotor, once reaches near bending subcritical speeds, the bifurcation phenomena is observed in the switching crack model for the increased level of unbalance. The bifurcation takes place to chaotic or quasi-periodic or subharmonic motion from period one motion. Rotors with high level of unbalance display rich form of quasi-periodic motion (Fig. 6). However, the rotor with lower level of unbalance shows chaotic and quasi-periodic nature at only limited speed values (Fig. 2(a)). Two kinds of bifurcations are noted, from periodic motion to chaotic or quasi-periodic and vice versa. This is because when rotor reaches near the subcritical speeds, the effect of abrupt stiffness switching due to opening and closing of the crack makes the response lose stability and becomes chaotic or quasi-periodic directly. The possible governing mechanism behind these bifurcation phenomena is the unstable stiffness switching while passing through the subharmonic resonance. Stronger the subharmonic resonance, more likely the bifurcation phenomena. Contrary to higher level of unbalance, rotors with low level of unbalance could quickly stabilize the vibration response, once it gets past the resonance and motion returns to period one.

The bifurcation phenomenon is not observed in case of breathing crack model (Figs. 4 and 8). Chaos, quasi-period and subsynchronous nature of the vibration motion is not seen for this crack model. The reason behind this could be the continuous gradual opening and closing of the crack. This makes the rotor lateral stiffness variation gradual. As a consequence, solution to the nonlinear equations always results in the stable period one response.

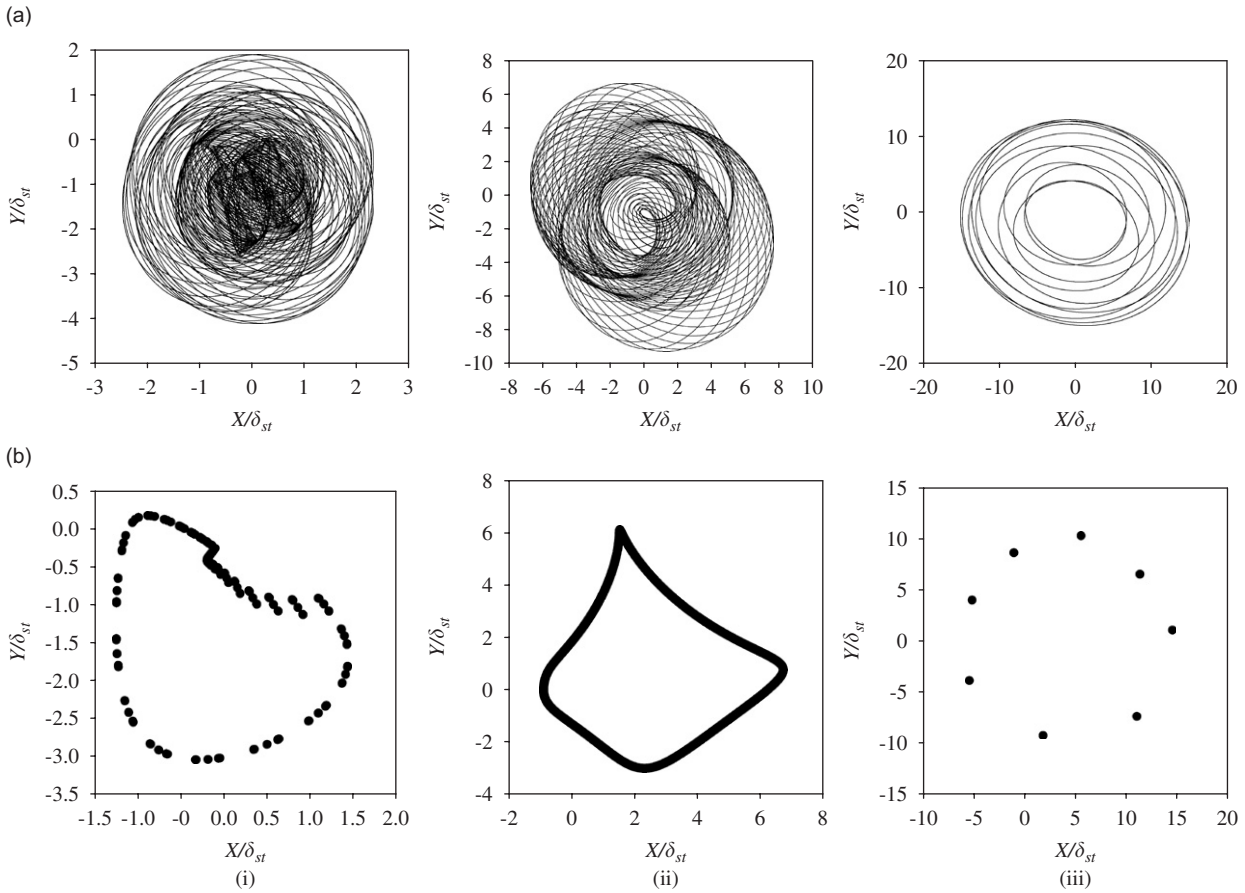

Fig. 7. (a) Orbit plots and (b) Poincaré maps at (i) $p = 0.316$, (ii) $p = 0.4699$, (iii) $p = 0.6735$; switching crack model, $a/D = 0.44$, $e = 4.0826$, $\beta = 90^\circ$.

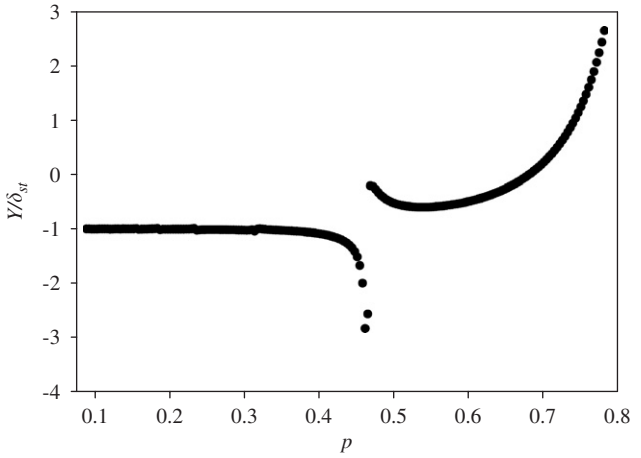

Fig. 8. Bifurcation diagram of breathing crack model, $a/D = 0.44$, $e = 4.0826$, $\beta = 90^\circ$.

3.2. Effect of unbalance orientation

The unbalance orientation angle is the angular position of the unbalance mass relative to the ξ axis (i.e. weak crack direction). Unbalance phase is very important parameter in the dynamics of the cracked rotor and a lot of studies [19,22] have been carried out to estimate its influence on the vibration response of cracked rotor. Hence it is important to understand its role on the nonlinear dynamics of the cracked rotor for both the crack models. Bifurcation diagrams of the cracked rotor system are shown in Fig. 9 ($a/D = 0.44$, $p = 0.482$, $e = 0.2042$) for both the crack models, using the unbalance orientation (β) as the control parameter. The unbalance angle β is varied from 0° to 360°, in the interval of 10°. Fig. 9(a) shows that eccentricity angle β has significant influence on the nonlinear behaviour of the cracked rotor modelled using switching crack model. There is quasi-periodic response for β value 0°. Poincaré map of Fig. 10(i) drawn for $\beta = 0^\circ$ reveals quasi-periodic nature of the motion. The rotor system enters the chaos at $\beta = 10^\circ$ and leaves the chaos at $\beta = 20^\circ$, where the rotor response becomes period 5. Response displays period one character of the vibration motion at subsequent unbalance angles, i.e. $\beta = 30^\circ$ and 40°. Rotor response becomes chaotic at next unbalance angle, and remains chaotic till $\beta = 90^\circ$. Fig. 10(ii) is Poincaré map for $\beta = 60^\circ$. The rotor enters into the quasi-periodic vibrations ($\beta = 110^\circ$ and 120°) via route of subharmonic vibrations (period 26), at $\beta = 100^\circ$. Vibration response returns to period one motion at $\beta = 130^\circ$. Next bifurcation is observed at unbalance angle 310°. An interesting behaviour is noticed at $\beta = 310^\circ$ (Fig. 10(iii)). The motion is not chaotic. The scattered attractors in the Poincaré map (Fig. 10(a)(iii)) are because of unstabilized motion even after sufficiently long time marching. Dense cluster of the points near the centre indicates that the motion is finally stabilized to few attractors. Poincaré map of Fig. 10(b)(iii) drawn for the last 1000 cycles indicate that motion is subharmonic with period 10. The system again enters into chaos at $\beta = 320^\circ$ and leaves the chaos through transient chaos at $\beta = 340^\circ$. Fig. 11 shows vibration response and Poincaré maps at $\beta = 340^\circ$. Fig. 11(b) is drawn using vibration data of first 750 cycles and Fig. 11(c) is drawn using data of remaining 2000 cycles. It can be noted from Fig. 11 that the chaotic motion died after approximately 750 cycles of rotation, response then stabilized in the period 4 motion. This transient chaos behaviour is observed for the first time in case of cracked rotor.

Fig. 12 ($a/D = 0.44$, $p = 0.626$, $e = 0.2042$) explains the bifurcation behaviour of the cracked rotor for both the crack models. The bifurcation diagram of switching crack model (Fig. 12(a)) shows quasi-periodic or subharmonic motion, when unbalance and crack directions are at or nearly perpendicular to each other (i.e. β is close to 90° or 270°). Fig. 12(a) indicates the rich quasi-periodic vibrations along with subharmonic vibrations at unbalance angles 60–140° and 250–290°.

Figs. 9(b) and 12(b) are the bifurcation characteristics of the cracked rotor using breathing crack model. The vibration motion is period one throughout the unbalance phase range (0–360°). Chaos and quasi-period nature determined in the response for the switching crack model are totally missing for the response obtained using breathing crack model.

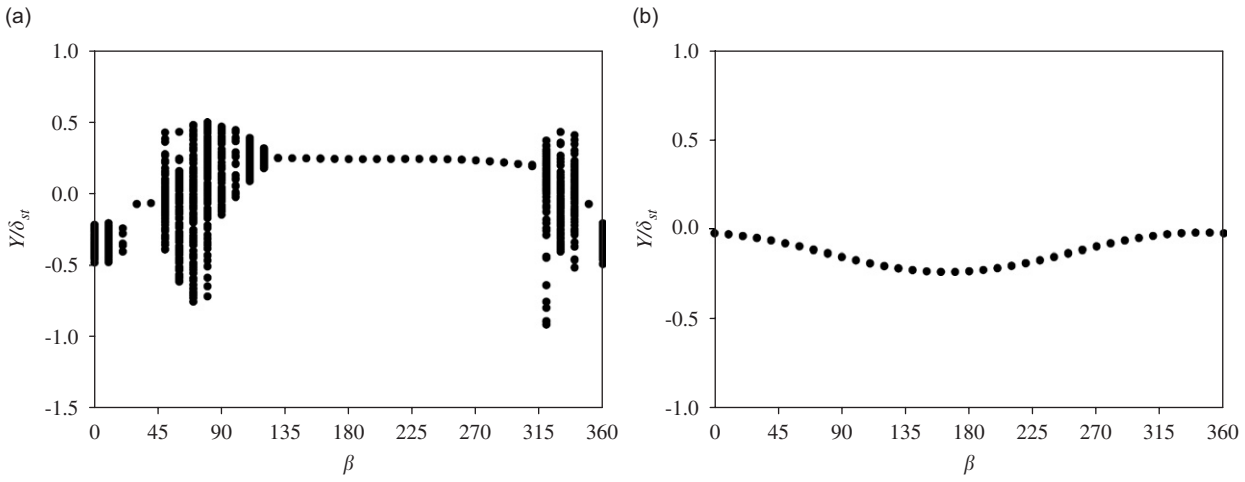

Fig. 9. Effect of unbalance orientation on bifurcation behaviour, $a/D = 0.44$, $p = 0.482$, $e = 0.2042$, $\beta = 0$–360°. (a) Switching crack model, (b) breaking crack model.

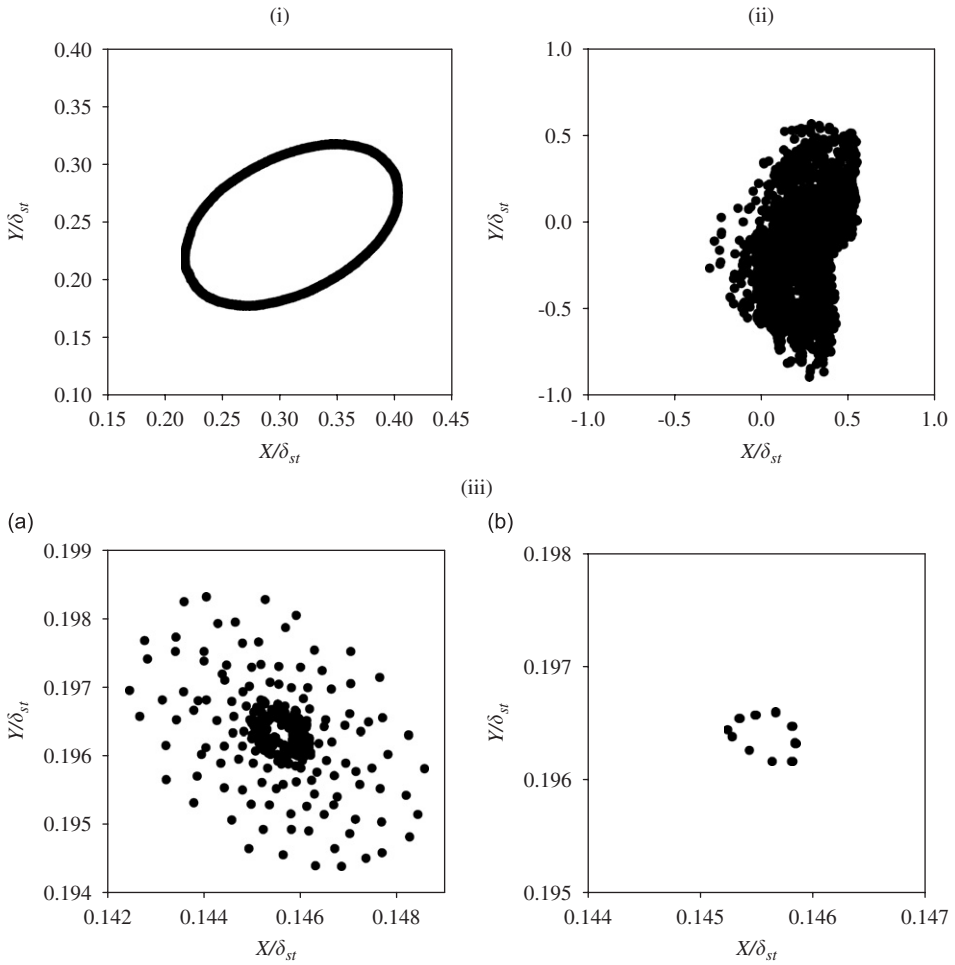

Fig. 10. Poincare maps with switching crack model, $a/D = 0.44$, $p = 0.482$, $e = 0.2042$, at (i) $B = 0$, (ii) $B = 60$, (iii) $B = 310$ (iii-a Using vibration data of all 3000 cycles, iii-b: using vibration data of last 1000 cycles).

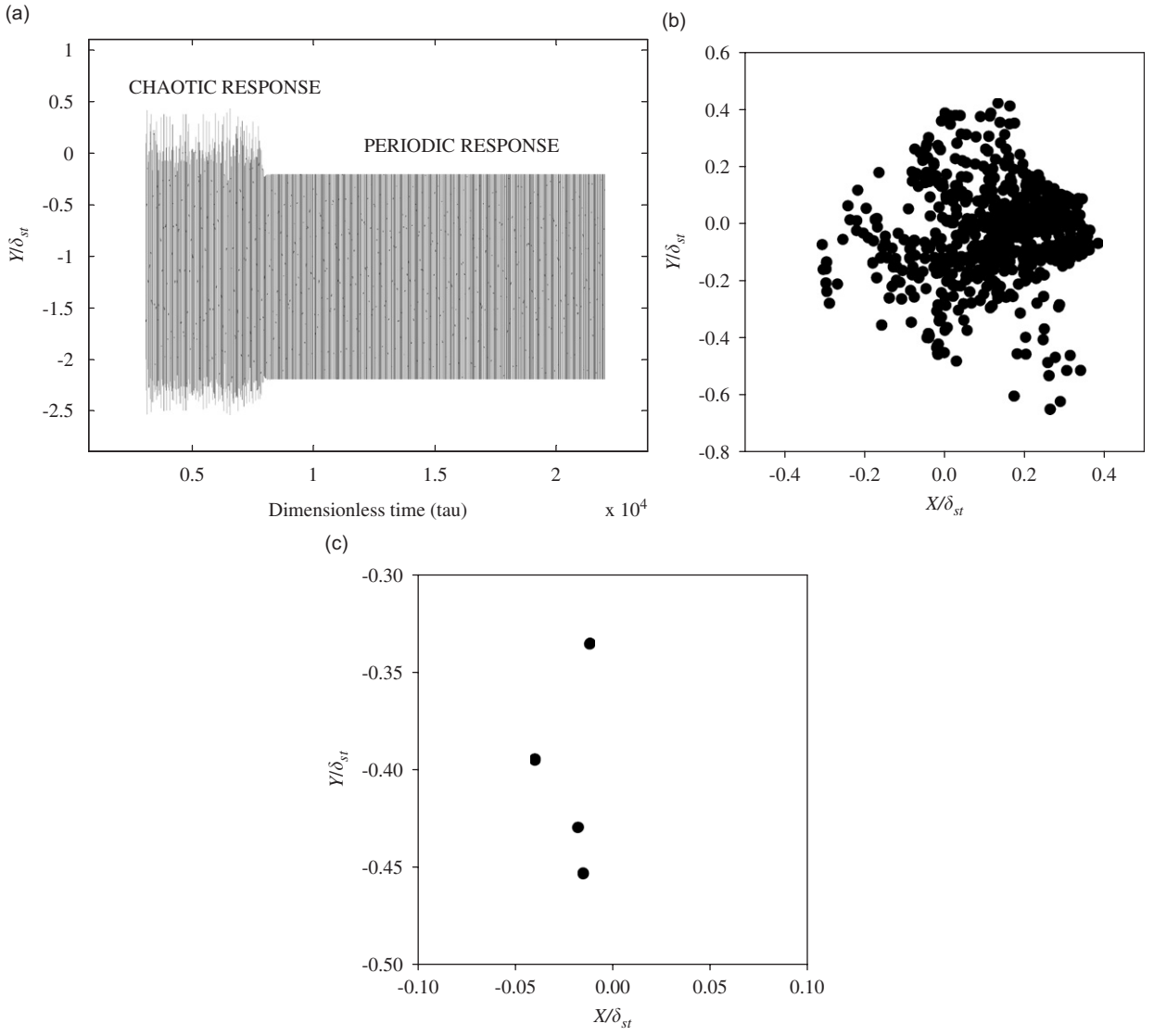

Fig. 11. (a) Vertical vibration response, (b) and (c) Poincaré maps at $\beta = 340^\circ$, switching crack model, $a/D = 0.44$, $p = 0.482$, $e = 0.2042$. (b) using vibration data of first 750 cycles, (c) using vibration data of last 1000 cycles.

3.3. Effect of crack depth

To study the effect of crack depth, bifurcation behaviour of both the crack models are found for the three crack depth ratios, i.e. $a/D = 0.44$, 0.35 and 0.2. In general, this crack depth ratio range covers most commonly encountered crack depths in practice. Nonlinear behaviour of the deeper cracked rotor, i.e. $a/D = 0.44$ has been investigated in detail in previous subsections, which indicate chaotic, quasi-periodic and subharmonic motion in the response of the switching crack model, at low level of unbalance. However, at higher unbalance level, the rotor shows rich form of quasi-periodic vibrations. It is important to recall that in case of breathing crack model, chaotic, quasi-periodic and subharmonic motions are completely absent in the response of the rotor. Dimensionless unbalance eccentricity of 4.0826 is taken for all subsequent simulations.

Fig. 13 explains the bifurcation phenomenon of the switching crack model at crack depth $a/D = 0.35$ drawn with speed ratio (p) as control parameter. Vibration response becomes quasi-periodic once rotor speed ratio crosses a value 0.4915. Switching crack model in this case experiences frequent bifurcations and the cracked

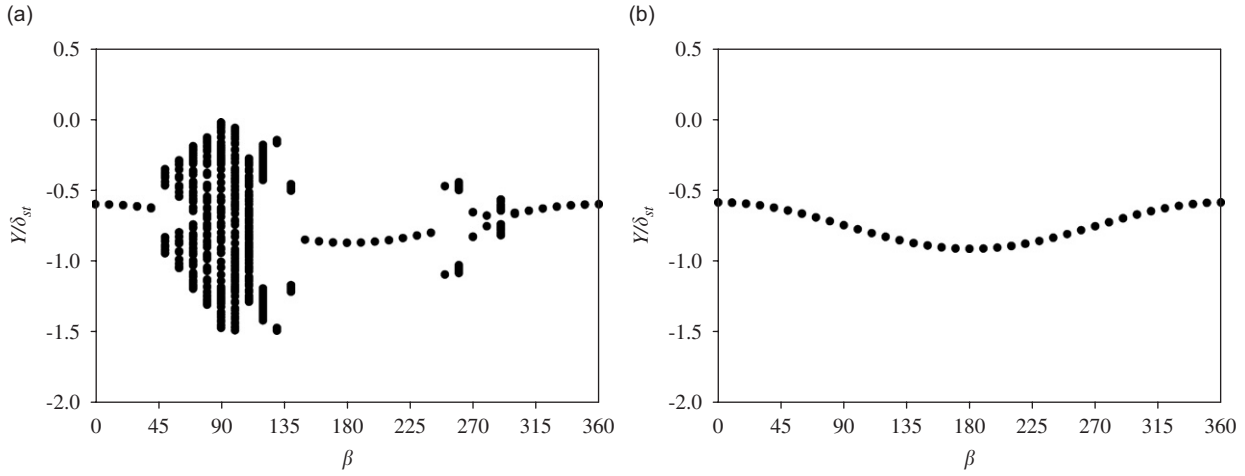

Fig. 12. Effect of unbalance orientation on bifurcation behaviour, $a/D = 0.44$, $p = 0.626$, $e = 0.2042$, $\beta = 0$–360°. (a) Switching crack model, (b) breaking crack model.

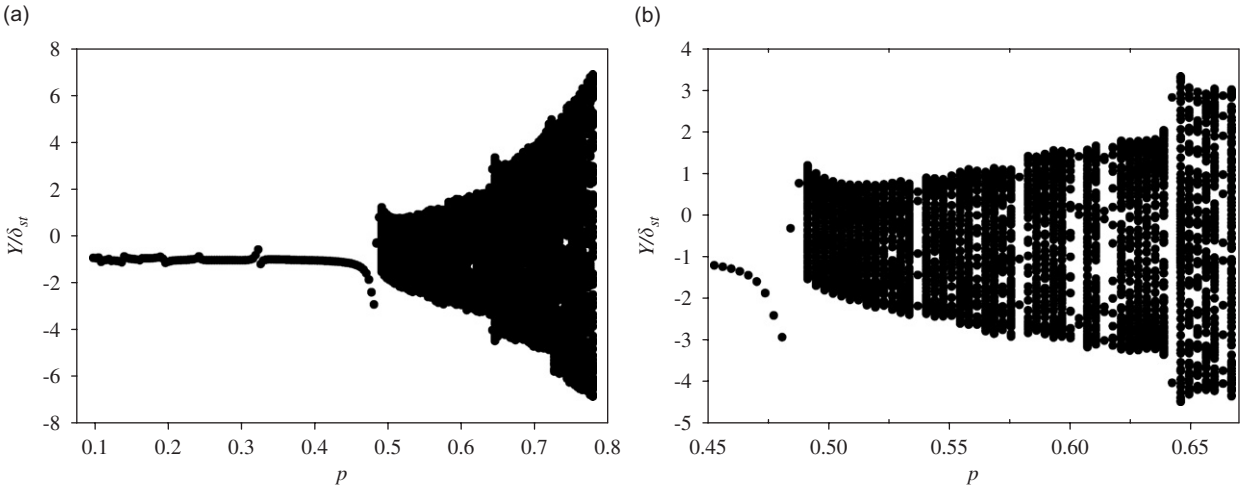

Fig. 13. Bifurcation diagram of switching crack model, $a/D = 0.35$, $e = 4.0826$, $\beta = 90^{\circ}$. (a) $p = 0.10$ to 0.78, (b) $p = 0.45$ to 0.67.

rotor exhibit rich quasi-periodic vibrations characterized by frequent appearance of periodic subharmonic orbits in between. For example, rotor response is periodic and subharmonic for $p = 0.5371$, 0.5792, 0.6143, 0.6178, 0.6635, 0.7231, 0.7407, 0.7688 and the respective periods are five, three, seven, sixteen, eleven, three, ten and four. Orbit plots and Poincaré maps of Fig. 14 reveal the nature of vibration response at some selected speed ratios. It is important to compare the nature of the vibration response of the switching crack model for the two crack depths, i.e. $a/D = 0.44$ and 0.35. Repeated occurrence of periodic subharmonic orbit found in case of $a/D = 0.35$ is not observed for $a/D = 0.44$. This means with reduction in the crack depth, the vibration motion is more likely to stabilize in periodic motion. Fig. 15 shows the bifurcation diagram of the cracked rotor using breathing crack model for the same rotor system parameters, which shows synchronous periodic motion, throughout the speed range.

Dynamic response of both switching and breathing crack models for shallow crack is simulated at crack depth ratio ($a/D = 0.2$). Figs. 16(a) and (b) are the bifurcation diagrams using switching and breathing crack models respectively. It can be noted that for low crack depths, both the models estimate nearly the same vibration characteristics. Chaotic, quasi-periodic and subharmonic vibrations are entirely missing from the response. The motion is period one throughout the speed range. This finding further strengthens the comment

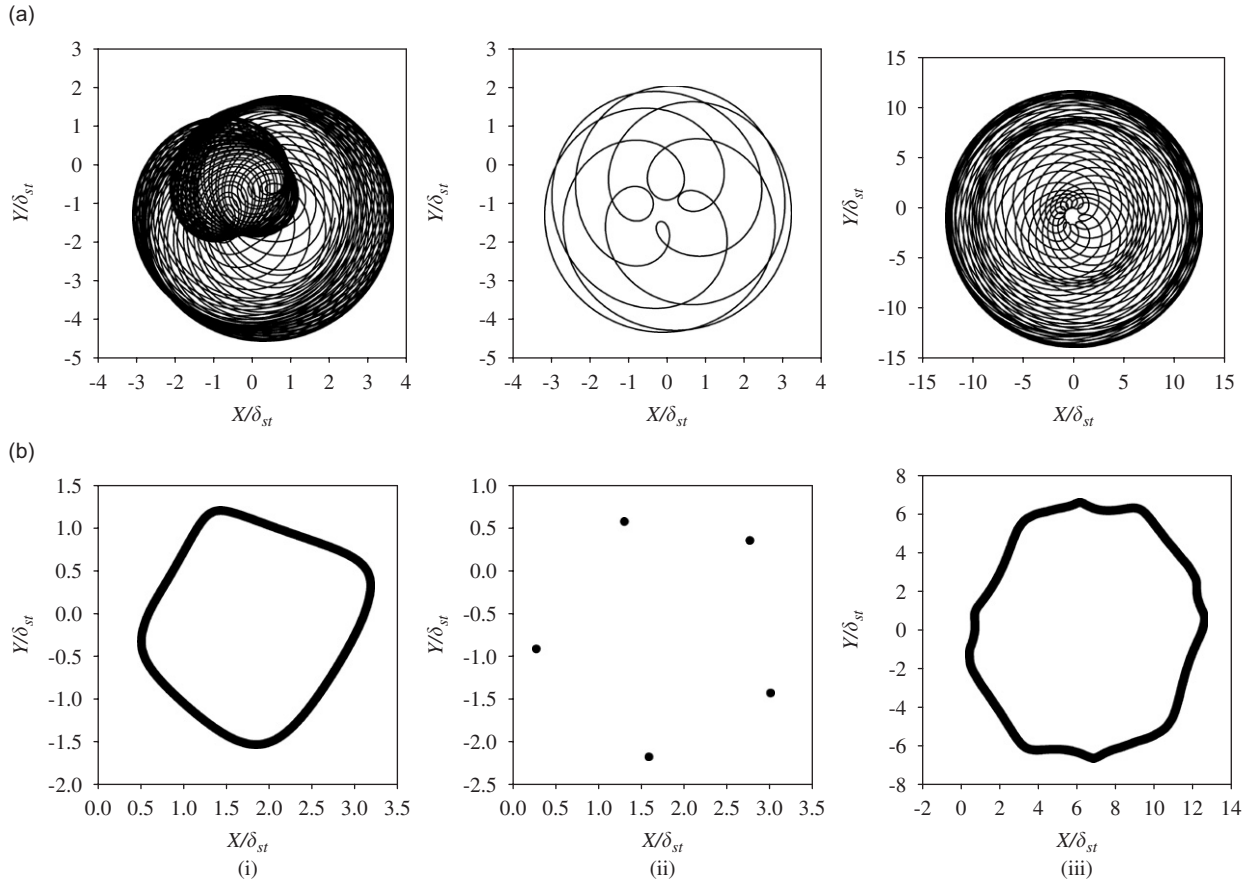

Fig. 14. (a) Orbit plots and (b) Poincaré maps at (i) $p = 0.4915$, (ii) $p = 0.5371$, (iii) $p = 0.7723$; switching crack model, $a/D = 0.35$, $e = 4.0826$, $\beta = 90^\circ$.

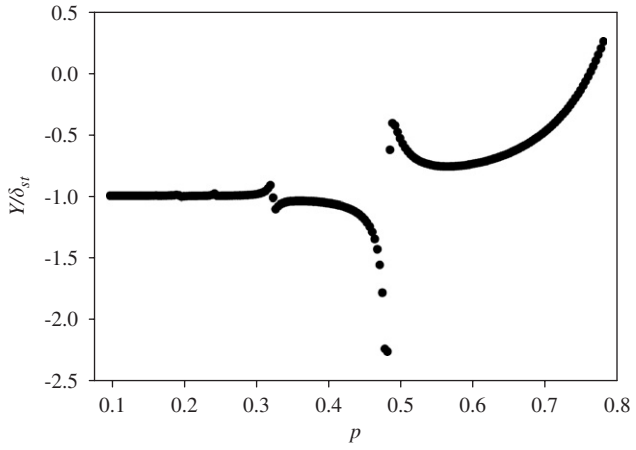

Fig. 15. Bifurcation diagram of breathing crack model, $a/D = 0.35$, $e = 4.0826$, $\beta = 90^\circ$.

made earlier regarding the role of crack depth in the bifurcation behaviour of the cracked rotor. With reduction in crack depth, vibration response is more likely to result in stabilized steady-state motion irrespective of the crack model used.

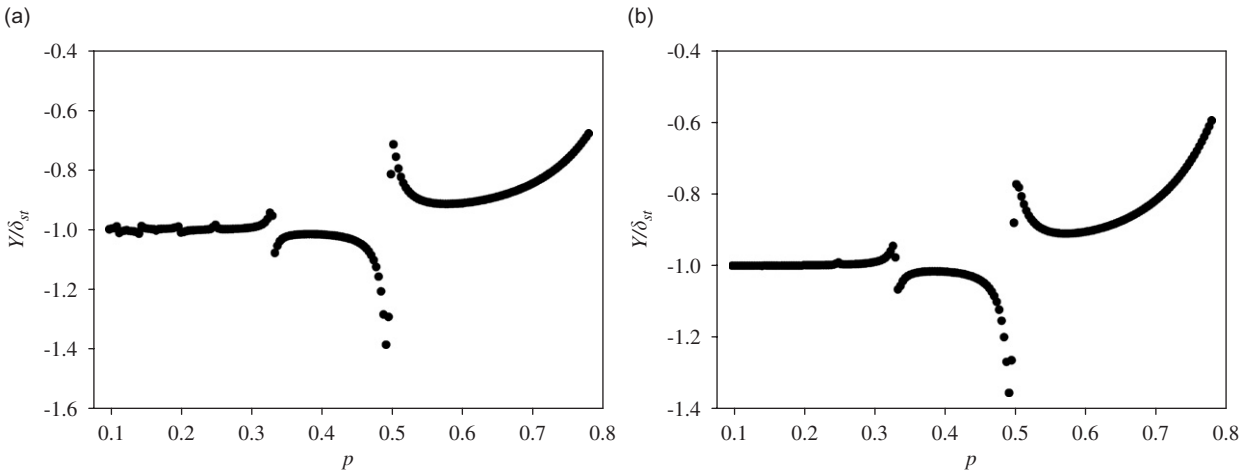

Fig. 16. Bifurcation diagram, $a/D = 0.20$, $e = 4.0826$, $p = 0.10$–0.78, $\beta = 90^\circ$. (a) Switching crack model, (b) breaking crack model.

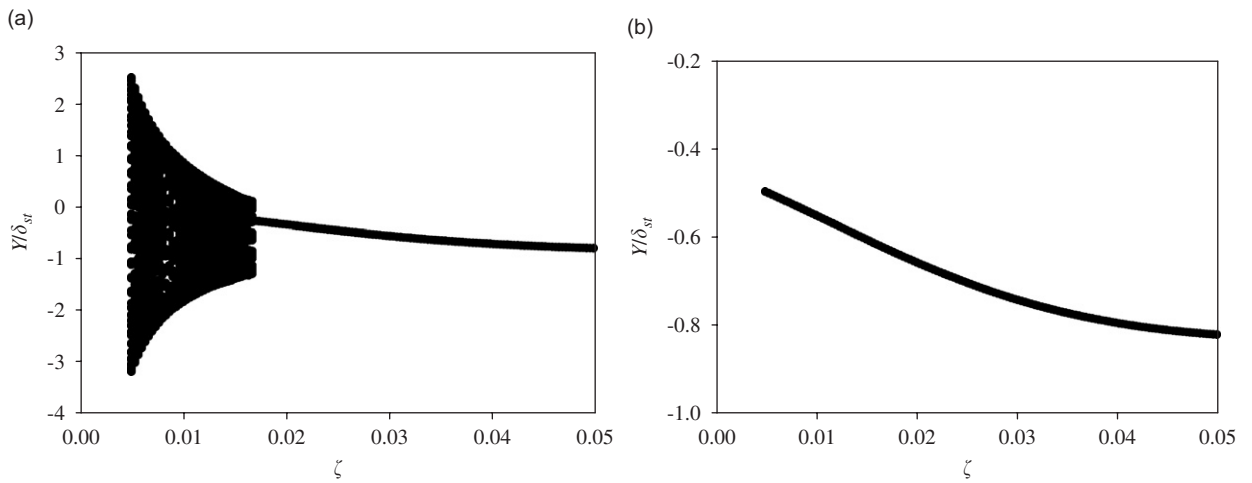

Fig. 17. Effect of damping on bifurcation behaviour, $a/D = 0.35$, $e = 4.0826$, $p = 0.5$, $\beta = 90^\circ$. (a) Switching crack model, (b) breaking crack model.

3.4. Effect of damping

Damping is another important rotor system parameter, which could greatly influence the nonlinear behaviour of the cracked rotor. The damping ratio ζ is increased in step of 3.352e−4 from 0.005 till $\zeta = 0.05$. The switching crack model indicates (Fig. 17(a)) quasi-periodic and subsynchronous motion until the damping value becomes $\zeta = 0.0168$. Response then onwards is periodic throughout. In case of breathing crack model, the bifurcation diagram reveals period one response for all damping values (Fig. 17(b)).

4. Conclusions

This study brings into focus, the modelling issue associated with crack breathing, when investigating nonlinear dynamics of the flexible cracked Jeffcott rotor on simple rigid supports. The work examines the nonlinear character of the cracked rotor in the subcritical speed range, using the two well-known crack models—switching crack and breathing crack, the former is most commonly used by researchers due to its

simplicity. Study covers crack depth ratios (a/D) equal to 0.2, 0.35 and 0.44. In this paper, the chaos and bifurcation phenomena are observed through numerical simulations for switching crack model and these phenomena are shown to be completely absent in case of breathing crack model. Effect of several important parameters has been investigated on the bifurcation characteristics of the rotor with switching crack. It is shown that unbalance phase, unbalance level, depth of crack and damping in the system have significant influence on the nonlinear vibration features of the cracked rotor with switching crack but have no influence on the rotor with breathing crack. For the rotors with deeper crack, the switching crack model displays chaotic, quasi-periodic and subharmonic motion. Chaos and quasi-period nature of the response is due to the unstable stiffness switching due to crack breathing in the rotor system. At low level of unbalance, the regions of chaos and quasi-period response are very small; on the other hand, the cracked rotor with higher level of unbalance exhibits rich form of quasi-periodic motion, with intermittent occurrence of subharmonic motion in between. Bifurcation phenomena observed in the switching crack model near the subcritical speeds can be attributed to the subharmonic resonance of the rotor. Stronger the resonance, more likely is the bifurcation phenomenon.

It has been shown for the first time that the phase of unbalance with respect to crack direction has significant effect on the bifurcation characteristics of the switching crack model. Depending upon the unbalance orientation, the response could be chaotic, quasi-periodic, subharmonic or period one. It is found that rotor with deeper cracked rotor modelled with switching crack model is likely to exhibit strong bifurcation phenomenon. Transient chaos behaviour is also observed for the first time in the case of cracked rotor with switching crack model. On the other hand, rotor with shallow crack reveals no bifurcation/quasi-periodic vibrations and this feature is same for both the crack models. Low value of damping results in chaos or quasi-periodic response.

The most significant outcome from the present study is that the chaotic, quasi-periodic and subharmonic vibrations are not observed in the response of the rotor with breathing crack model for the similar set of parameters as used for switching crack model. It is important to note that since the breathing crack model accounts for the forces acting on the crack cross-section and thereby evaluate the open-close area of crack, and in turn estimate the shaft stiffness, the breathing crack model is expected to more closely represent the breathing of cracks in real rotors, rather than the switch ON and switch OFF kind of model (switching crack model). Through the present study it is shown that the chaotic and quasi-periodic vibrations reported in the past for cracked rotor could be due to the mathematical approximation model of the crack breathing. It may also be important to note that the kind of chaotic, quasi-periodic and subharmonic response found using switching crack model, is not observed experimentally by researchers [2,3,10]. Hence, switching crack model should be used with care to predict the vibration characteristic of the cracked rotor; particularly for deeper cracks. The model is easier to implement mathematically and yields rich nonlinear dynamic response features, as shown in this paper and claimed by some researchers in the past. However, these vibration features could only be due to specific mathematical model used in the simulation and may not be observed in practice.

References

[1] R. Gasch, A survey of the dynamic behaviour of a simple rotating shaft with a transverse crack, *Journal of Sound and Vibration* 160 (1993) 313–332.
[2] A.D. Dimarogonas, Vibration of cracked structures: a state of art review, *Engineering Fracture Mechanics* 55 (1996) 831–857.
[3] G. Sabnavis, R.G. Kirk, M. Kasarda, D. Quinn, Cracked shaft detection and diagnostics: a literature review, *The Shock and Vibration Digest* 36 (2004) 287–296.
[4] I. Imam, S.H. Azzaro, R.J. Bankert, J. Scheibel, Development of an on-line rotor crack detection and monitoring system, *Journal of Vibration, Acoustics, Stress and Reliability in Design* 111 (1989) 241–250.
[5] T. Zhou, Z. Sun, J. Xu, W. Han, Experimental analysis of cracked rotor, *Journal of Dynamical Systems, Measurements, and Control* 127 (2005) 313–320.
[6] O.S. Jun, H.J. Eun, Y.Y. Earmme, C.W. Lee, Modelling and vibration analysis of a simple rotor with breathing crack, *Journal of Sound and Vibration* 155 (1992) 273–290.
[7] J.J. Sinou, A.W. Lees, The influence of cracks in rotating shafts, *Journal of Sound and Vibration* 285 (2005) 1015–1037.
[8] C.A. Papadopoulous, A.D. Dimarogonas, Coupled vibrations of cracked shafts, *Journal of Vibration and Acoustics* 114 (1992) 461–467.

[9] W.M. Ostachowicz, M. Krawczuk, Coupled torsional and bending vibrations of a rotor with an open crack, *Archive of Applied Mechanics* 62 (1992) 191–201.
[10] A.K. Darpe, K. Gupta, A. Chawla, Coupled bending, longitudinal and torsional vibrations of a cracked rotor, *Journal of Sound and Vibration* 269 (2004) 33–60.
[11] D.D. Quinn, G. Mani, M. Kasarda, T. Bash, D.J. Inmam, R.G. Kirk, Damage detection of a rotating cracked shaft using an active magnetic bearing as a force actuator—analysis and experimental validation, *ASME Transactions of Mechatronics* 10 (2005) 640–647.
[12] P. Muller, J. Bajkowski, D. Soffker, Chaotic motions and fault detection in a cracked rotor, *Nonlinear Dynamics* 5 (1994) 233–254.
[13] J. Pu, J. Chen, J. Zou, P. Zhong, The research on nonlinear characteristics of cracked rotor and reconstruction of crack forces, *Proceedings of Institution of Mechanical Engineers, Journal of Mechanical Engineering Science* 216 (2002) 1099–1108.
[14] J. Pu, J. Chen, J. Zou, P. Zhong, Quasi-periodic vibration of cracked rotor on flexible bearings, *Journal of Sound and Vibration* 251 (2003) 875–890.
[15] W. Qin, G. Meng, T. Zhang, The swing vibration, transverse oscillation of cracked rotor and the intermittence chaos, *Journal of Sound and Vibration* 259 (2003) 571–583.
[16] W. Qin, G. Meng, R. Xingmin, Grazing bifurcations in the response of cracked Jeffcott rotor, *Nonlinear Dynamics* 35 (2004) 147–157.
[17] F. Yiming, Z. Yufang, Z. Shijian, Analysis of the chaotic motion for the rotor system with transverse crack, *Acta Mechanica Solida Sinica* 16 (2003) 74–80.
[18] R. Gash, Dynamic behaviour of a simple rotor with cross sectional crack, Transactions of Institution of Mechanical Engineers, *International Conference on Vibration in Rotating Machinery*, paper C178/76, Cambridge, UK, 15–17 September 1976, pp. 123–128.
[19] A.K. Darpe, K. Gupta, A. Chawla, Transient response and breathing behaviour of the cracked Jeffcott rotor, *Journal of Sound and Vibration* 272 (2004) 207–243.
[20] A.K. Darpe, K. Gupta, A. Chawla, Analysis of the response of a cracked Jeffcott rotor to axial excitation, *Journal of Sound and Vibration* 249 (2002) 429–445.
[21] H. Tada, P.C. Paris, G.R. Irwin, *The Stress Analysis of Crack Handbook*, Del Research Corporation, Hellertown, PA, 1973.
[22] J. Schmied, E. Kramer, Vibrational behaviour of a rotor with a cross sectional crack, *Proceedings of Institution of Mechanical Engineers, Journal of Mechanical Engineering Science* 195 (1984) 57–73.